International Journal of Heat and Mass Transfer 79 (2014) 279–290

Contents lists available at ScienceDirect

International Journal of Heat and Mass Transfer

journal homepage: www.elsevier.com/locate/ijhmt

Taylor bubble-train flows and heat transfer in the context of Pulsating Heat Pipes

Balkrishna Mehta, Sameer Khandekar *

Department of Mechanical Engineering, Indian Institute of Technology Kanpur, Kanpur 208016, UP, India

ARTICLE INFO

Article history:
Received 12 May 2014
Received in revised form 17 July 2014
Accepted 5 August 2014

Keywords:
Pulsating Heat Pipes
Taylor bubble flow
Bubble slip
Local Nusselt number
Heat transfer enhancement

ABSTRACT

Understanding the performance of Pulsating Heat Pipes (PHPs) requires spatio-temporally coupled, flow and heat transfer information during the self-sustained thermally driven flow of oscillating Taylor bubbles. Detailed local hydrodynamic characteristics are needed to predict its thermal performance, which has remained elusive. Net heat transfer in PHP is contributed by (a) pulsating/oscillating flow (b) distribution of different liquid slugs and bubbles, and, (c) phase-change process; however, its contribution is minimal. In fact, the former two flow conditions are largely responsible for heat transfer in PHPs; such flow conditions can be generated without phase-change and can also be studied independently to observe their explicit effects on PHP heat transfer. With this motivation, systematic experimental investigation of heat transfer is performed during (a) isolated Taylor bubble flow (b) continuous Taylor bubble flow and (c) pulsating Taylor bubble flow, at various frequencies (1 Hz to 3 Hz, as applicable for PHPs) inside a heated square mini-channel of cross-section size 3 mm × 3 mm. This study clearly reveals important insights into the PHP operation. Oscillating Taylor bubbles create significant disturbances in their wake which leads to local augmentation of sensible heat transfer. The implications of bubble length, wake characteristics, oscillating frequency and bubble slip velocity on the heat transfer augmentation and, in turn on thermal performance of PHPs can be clearly delineated from this study. The study also brings out the nuances in the estimation of true bubble slip under time varying Taylor bubble flows.

1. Introduction

With the advances in mini/micro fabrication techniques, many applications have emerged which utilize or involve single-phase as well as two-phase non-pulsating and pulsating flows, respectively, in such mini/micro geometries. Finding and delineating transport mechanisms in such systems is a major challenge and research impetus has greatly increased in this direction so as to achieve mini-/microscale systems with better control and improved efficiency. One such device, which utilizes self-excited thermally driven two-phase flow oscillations for enhanced passive heat transfer is a Pulsating Heat Pipe (PHP), also referred to as an Oscillating Heat Pipe (OHP). This device has attracted considerable research in recent past due to its simplicity, ease of manufacture and versatility; however the flow and heat transfer phenomena in this device is quite complex and intriguing. The transport mechanisms of this 'simple' device also pose an excellent opportunity to understand its complex internal two-phase thermo-hydrodynamics, i.e., thermo-hydrodynamics of pulsating/oscillating slug flow or Taylor bubble-train flow in capillaries [1–5].

In PHPs, bubbles act as pumping elements, transporting the entrapped liquid slugs in a complex oscillating–translating–vibratory fashion, resulting in self-sustained thermally driven flow oscillations, thereby ensuing highly efficient passive heat transfer. In addition to the latent heat, considerable amount of sensible heat transfer also occurs in a PHP, i.e., Taylor slug-bubble train flow under pulsating/oscillating condition and the resulting liquid slug-bubble distribution contributes significantly to the net heat transport. The primary motivating factor for initiating the present work reported here is to eventually help understand the complex self-induced thermally driven oscillatory flow encountered in Pulsating Heat Pipes. The actual flow patterns and heat transfer mechanisms in a PHP are too intricate as they simultaneously depend on many parameters such as applied thermal gradient, thermo-physical properties of the working fluid and filling ratio. The local heat transfer also depends on bubble velocity, bubble shapes, surface wettability, liquid film thickness surrounding the bubble, oscillating frequency and evaporation at the interface, etc. This multitude of interwoven factors makes it very difficult to analyze this device.

* Corresponding author. Tel.: +91 512 259 7038; fax: +91 512 259 7408.
E-mail address: samkhan@iitk.ac.in (S. Khandekar).

http://dx.doi.org/10.1016/j.ijheatmasstransfer.2014.08.005
0017-9310/

Nomenclature

A	area of cross section (m^2)
C_p	specific heat at constant pressure (J/kg K)
D_h	hydraulic diameter (m)
Δf	number of frames (–)
h	heat transfer coefficient (W/m^2 K)
J	superficial velocity (m/s)
k	thermal conductivity (W/m K)
ℓ	length specified in image (m)
L	length of the channel, characteristic length (m)
m	ratio of relative velocity to bubble velocity (–)
N	number of bubble observations (–)
n	frame capture rate (s^{-1})
Q	volumetric flow rate (m^3/s)
R	radius (m)
q''	heat flux (W/m^2)
t	time (s)
T	temperature (K)
T^*	non-dimensional temperature $\left(=\frac{\bar{T}-T_{fi}}{(q''\cdot D_h)/k_l}\right)$
U	velocity (m/s)
Z	distance from inlet (m)
Z^*	thermal non-dimensional distance (=$Z/Re\cdot Pr\cdot D_h$)

Greek symbols

α	thermal diffusivity (m^2/s)
β	volume flow ratio (–)
δ	liquid film thickness (m)
γ	frequency of oscillation (Hz)
μ	dynamic viscosity (Pa s)
ρ	mass density (kg/m^3)
θ	time period
ψ	ratio of bubble velocity to total superficial velocity (–)
σ	surface tension (N/m)

Non-dimensional numbers

Ca	Capillary number ($\mu_l\cdot U_b/\sigma_l$)
Nu	Nusselt number ($h\cdot D_h/k_l$)
Pr	Prandtl number (υ/α)
Re	Reynolds number ($\rho_l\cdot J_l\cdot D_h/\mu_l$)
St	Strouhal number ($\gamma\cdot D_h/U_{avg}$)
We	Weber number ($\rho_l\cdot U_b^2\cdot D_h/\sigma_l$)

Subscripts

b	bubble, bulk
f	fluid
$f-i$	fluid inlet
g	gas
h	hydraulic, hydrodynamic
l	liquid
s	slug
tot	total
uc	unit cell
w	wall

Hence, as on date, there is no complete mathematical model available for predicting the thermal performance of a PHP.

In this background, analyzing the PHP problem by splitting it into several simple problems and eventually coupling it later for a comprehensive description will be a logical and practical step ahead. One way of splitting the complex problem is as follows:

- Hydrodynamics of isolated Taylor bubble and continuous Taylor bubble-train flow of two-component two-phase systems can be investigated in the mini-channels, during upward, downward and horizontal configurations. No heat transfer and phase-change is involved in this analysis.
- External pulsations of different frequencies are added to continuous Taylor bubble-train, which will make the Taylor bubble system to pulsate and effect of pulsations on hydrodynamics is studied.
- After studying the hydrodynamics, parametric study of heat transfer of these systems is analyzed without phase-change.
- Finally, phase-change can be incorporated in the Taylor bubble flow to map the flow with the functioning of real time PHPs.

Motivation for taking up this study also arises from the fact that the subject of oscillating/pulsating motion of liquid slugs inside mini/micro-channel (or through pipes, capillary tubes, etc.) has received attention over the last two decades, both due to the large number of practical mini/microscale applications in which it appears and interesting scientific challenges it poses. The oscillations may be externally controlled, thermally driven or alternatively, they may arise due to the effect of the dynamic instabilities which are inherent part of two-phase boiling/condensation systems [7,8]. In unidirectional steady flow situations, momentum diffusion time is the only relevant time scale. However, in oscillatory/pulsating systems, in contrast, the flow is characterized by a second imposed time scale that is due to the applied pressure gradient; hence, the transport characteristics of the resulting flow depend on the ratio of the diffusion time to the imposed time scale, i.e., Strouhal number (St). The magnitude of St determines the importance of acceleration effect in the fluid relative to the viscous diffusion of momentum. In this role, it is evident that St can be qualitatively compared to Reynolds number, based on a characteristic 'velocity' $\sim\gamma\times D$. In addition, during oscillatory flows, the velocity of the meniscus/bubble continuously changes, resulting in dynamic variation of Re, Ca, We, etc.

In the context of PHPs, the effect of the film evaporation has been clearly highlighted by models proposed by Zhang and Faghri [5]. More recently Das et al. [9] and Rao et al. [10] have provided a detailed description of the effect of the thin film properties on PHP dynamics. Zhang and Faghri [5] showed that a part of the heat transfer is due to evaporation and condensation of the working fluid, i.e., by latent heat. Another part is due to heat transfer between the tube wall and liquid slugs in the form of single-phase heat transfer, i.e., sensible heating. As an outcome, the authors showed that more than ~90% of total heat is transferred by sensible heating. Therefore, the heat transfer problem of a PHP can be studied by breaking it into two logical sub-divisions, i.e., (i) latent heat trough the thin film evaporation or by nucleate boiling (at high heat fluxes), and, (ii) sensible heat transfer which is brought about by the motion of liquid slugs trapped between Taylor bubbles. The arguments by Zhang and Faghri [5,6], supported by complementary studies by others e.g., Khandekar and Groll [3] and Das et al. [9], clearly highlight the importance of sensible heat as the primary mechanism of heat transfer.[1] In this background, understanding of thermal-fluidic transport during non-boiling steady and pulsating Taylor-flows gains importance.

[1] Nevertheless, it must be noted that bubbles and associated latent heat transfer through the thin film is indeed required for the self-sustained oscillatory flow inside a PHP. This rapid vapor addition in the heater zone (so also, condensation in the cold zone) lead to flow oscillations, which eventually drive the adjoining liquid slugs between the heated and the cold end, resulting in the associated large sensible heat transfer through their movement.

Very few quantitative studies are available describing controlled oscillatory flows under heated conditions. Das et al. [9] have recently undertaken a parametric study of a two-phase oscillating flow in a capillary tube. Their experimental system represents the simplest version of a PHP; it consisted of a capillary tube of ID = 2 mm connected between two reservoirs with pentane as the working fluid. Experiments were performed at different operating pressures. Visualization was performed and the oscillations of the isolated liquid–vapor meniscus inside the capillary tube and the corresponding variation of local pressure were observed. It was found that such a system could develop instability that leads to thermally driven meniscus oscillations, as observed in a multi-turn PHP device. In another subsequent study by Rao et al. [10], an attempt was made to explain the self-sustained thermally-induced meniscus oscillations observed by Das et al. [9]. A unique and novel understanding of the system dynamics was achieved by real-time synchronization of the internal pressure measurement with high-speed videography. It was outlined that contact angle hysteresis at the three-phase meniscus contact line during its upward and downward stroke plays a significant role in local evaporation and condensation dynamics. However, this study did not quantify the extent of sensible heat transfer during the self-sustained oscillatory meniscus motion between the hot and cold zones.

There are many studies available in the literature where the mechanically generated Taylor bubble flow has been studied from the flow behavior perspective (mimicking the PHP flow pattern, however without thermal effects). Study of heat transfer during the continuous Taylor bubble-train flow (non-boiling, two-component air–water systems) has also attracted attention due to its heat transfer enhancement capabilities. Many numerical and experimental studies have shown that when low density Taylor bubbles slip through the liquid slugs, they modify the flow field inside the slugs [11–20]. This modification of the flow field in terms of recirculation inside the liquid slugs enhances the local mass, momentum and energy transport near the meniscus [18]. This, in turn, increases the heat transfer capability as compared to the single-phase flow [19–26].

Extension of purely adiabatic Taylor bubble-train flow situations to diabatic conditions (with heat transfer), with and without externally applied pulsations is a logical step forward to discern the complex local transport phenomena. One way to generate pulsating Taylor bubble-train flow in a mini-/micro channel is by injecting gas bubbles in the pulsating liquid flow. As for the case of continuous Taylor bubble-train flow, flow distribution and oscillating frequency of liquid slugs and bubbles is expected to play an important role in heat transport. Thus, in pulsating Taylor bubble-train flow, externally imposed frequency of pulsating liquid will add another parameter. As has been noted earlier, this phenomenon is qualitatively similar to the flow mechanism found in Pulsating Heat Pipes (PHPs). Certainly, there is no phase-change and chaotic movement of slug-vapor bubbles involved as found in PHPs, which makes the latter system quite complex. In comparison to PHPs, pulsating Taylor bubble-train systems are simpler but independent study of hydrodynamics and heat transfer of this kind of systems is likely to contribute in better understanding of PHP systems. To the best of our knowledge, there are no explicit studies available in open literature related to pulsating Taylor bubble-train flows.

Hence, in line with the global motivation of understanding the complex flow and heat transfer in Pulsating Heat Pipe systems, in this work, IR Thermography of isolated Taylor bubble flow, continuous Taylor bubble-train flow and pulsating Taylor bubble-train flow, has been undertaken. This study presents the experimental investigations of (a) Local thermal footprints of an isolated Taylor bubble flow in a one side heated square mini-channel of cross-section 3.0 mm × 3.0 mm for different bubble lengths compared to the heated length (b) Local heat transfer measurements of pulsating Taylor bubble-train flow in the channel of cross-section 3.0 mm × 3.0 mm, for different frequencies and total superficial velocity (J_{tot}) ranging from 1 Hz to 3 Hz and 0.11 m/s to 0.15 m/s, respectively. These conditions are inline with what is usually found in a typical Pulsating Heat Pipe system [27–29]. Augmentation/deterioration in heat transfer, as compared to continuous Taylor bubble-train flow, is also presented.

2. Experimental set-up and data reduction

Schematic of experimental set-up for performing the above mentioned heat transfer study is shown in Fig. 1. As the flow and heat transfer is transient in nature, design of set-up was done such that, the transient temperature profile of the heated wall could be successfully captured. With the aim of measuring heat transfer during two-phase Taylor flows, thickness and wall material were chosen, not only to satisfy the Biot number criterion for a lumped system, but also to have high Fourier number for getting very low diffusion time scale of the heater. A square channel with a T-junction assembly of cross-section size 3.0 mm × 3.0 mm was machined on 500 mm × 250 mm × 12 mm polycarbonate substrate, as shown. Length of the two-inlet channel sections before reaching to the T-junction were kept as 165 mm and 200 mm. After the T-junction, an unheated length of 110 mm was provided for the complete hydrodynamic development of the flow under the entire range of applicable flow Reynolds numbers. The heated length was kept as 125 mm and another unheated 65 mm length was provided after the heater in the downstream direction to minimize the outlet end effects in the heated test section. The T-junction assembly was provided to facilitate the generation of two-phase Taylor bubble flow. The heater was made of 70 μm thin Stainless steel strip of size 150 mm long and 4 mm wide, which was bonded over the polycarbonate plate with a milled square channel such that the heater strip itself acted as the fourth wall of the channel. Diffusional time scale of the heater wall was equal to 1.460×10^{-3} s, which gave sufficiently high value of *Fo* during the entire range of flow pulsations. The strip was heated by Joule heating using a high current DC power supply (V: 0–60 V and I: 0–50 A) which ensured a constant heat flux thermal boundary condition (typically of the order of 1.0 W/cm^2). To provide fluctuations in the flow, two solenoid valves (Make: Burkert®; time response: 50 ms), one each for water and air, respectively, were operated by an electronic controllable timer circuit. Transient flow profile was captured by an electronic flow meter (Cole-Parmer® LF series, response time: 20 ms, voltage output: 0–5 V, flow rate: 0–100 ml/min).

During the series of experiments, two data acquisition cards from National Instruments®, NI 9213, 24 bit resolution, 1200 S/s, 16 channel temperature module and NI cDAQ 9172 with NI 9205, 16 bit resolution, 250 kS/s, 16 channel voltage module, were used to acquire the temperature and voltage data, respectively. National Instruments® Labview-2009 software was used to interface the hardware with the computer. In the present experiments, both temperature and voltage data were acquired at 30 Hz. For visualization of the Taylor bubbles, Photron-Fastcam®-SA3 120 K high-speed camera was used at 1000 fps and 1024 × 1024 pixel resolution.

For obtaining the complete temperature field of heated wall in the experiments, FLIR® ThermoVision SC 4000 MWIR InfraRed camera was used. Acquisition of images and post-processing was done by using ThermaCAM® Researcher-V2.9 software. IR images were also acquired at 30 Hz. The IR camera was equipped with an Indium Antimonide detector array and had an operational spectral band of 3–5 μm, 14 bit signal digitization, spatial resolution of 320 (H) × 256 (V) and a Noise Equivalent Temperature Difference of less than 0.02 K at 30 °C. For measuring the fluid bulk mean mixing temperature at the inlet and the outlet cross-section, two K-type micro-thermocouples (Make: Omega®, Bead diameter:

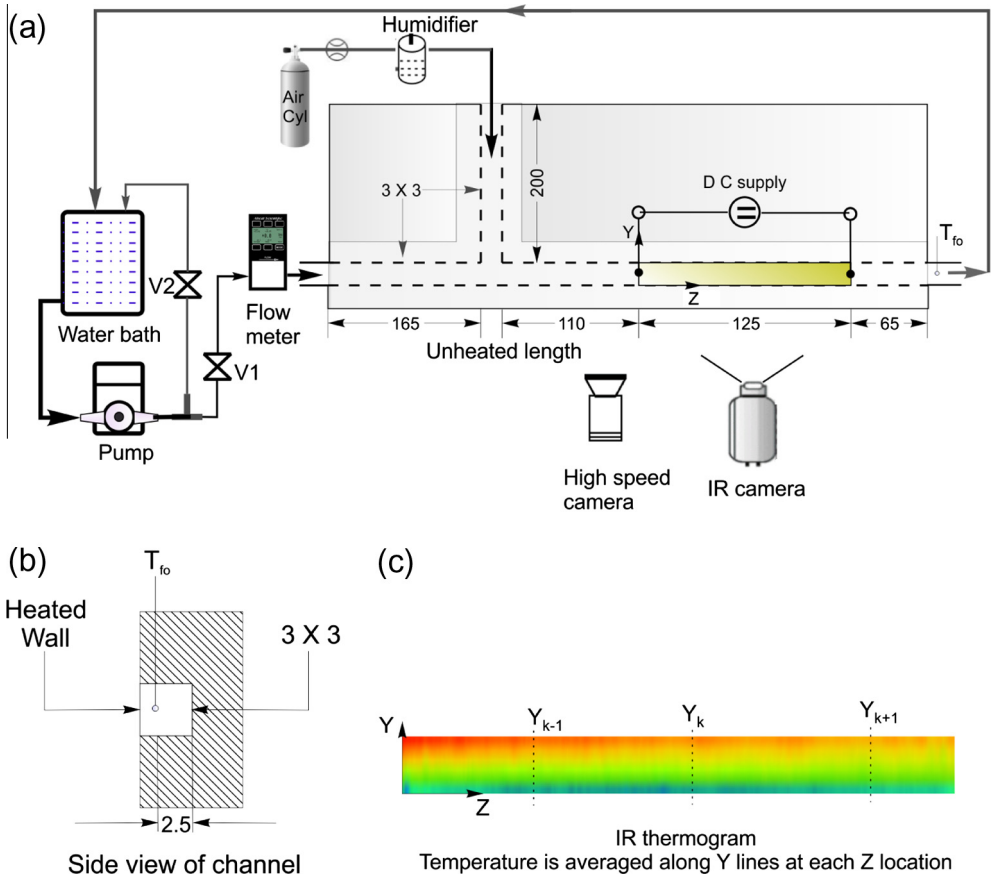

Fig. 1. (a) Schematic and dimensional details of the experimental set-up and visualization arrangements, (b) shows the details of the channel cross-section and (c) shows a typical IR thermograph of the heated channel wall; the scheme for transverse averaging (along *Y*-direction) of the local wall temperature at any given location in the flow direction (*Z*) is shown.

0.13 mm) were used. The intermediate fluid temperatures at various axial locations were estimated by linear interpolation of these two measured thermocouple values. Uncertainties estimated in the measurement of wall and fluid temperatures were not more than 7% and 5%, respectively. Estimation of non-dimensional temperatures, Nusselt number and bubble velocity are estimated by using the raw data and given below.

The values of fluid and wall temperature (recorded by micro-thermocouples and IRT, as the case may be) are non-dimensionalized as follows:

$$T^* = \frac{\bar{T} - \bar{T}_{f-i}}{(q'' \cdot D_h)/k_s} \tag{1}$$

where, $\bar{T} = \bar{T}_f$ or $\bar{T}_w$ as per the case; applied q'' and $\bar{T}_{f-i}$ being specified for a given run.

The local, time averaged Nusselt number along the flow direction is defined as:

$$(Nu_z)_{ta} = \frac{q''_z \cdot D_h}{(\bar{T}_w - \bar{T}_f) \cdot k_f} \tag{2}$$

where, q''_z is the local flux at the desired location along the flow direction and, $\bar{T}_f$ = local fluid temperature along the axial direction inside the channel, which is obtained by a linear interpolation of the inlet and outlet bulk mean mixing temperature, respectively. $\bar{T}_w$ = local time averaged wall temperature at any given location obtained by IRT along the *Z*-axis (flow direction), averaged along the direction of *Y*-axis (transverse direction), over the front face of the channel wall (as shown in Fig. 1(c)).

Mean bubble velocities are calculated from digital analysis of images obtained from high-speed videography. As image acquisition rate is known, bubble velocity can be ascertained. For example, if N is the number of bubbles tracked for estimating the average bubble velocity U_b, n represents the fame rate of video capture, ℓ represents the length of the observation window and Δf is the number of frames required for a bubble to pass through the window, then average bubble velocity U_b is given by:

$$U_b = \frac{1}{N}\sum_{i=1}^{N}\left(\frac{\ell}{\Delta f}\right)_i n \tag{3}$$

Slip ratio of the bubbles at the interface is calculated as:

$$\psi = (U_b/J_{tot}) \tag{4}$$

It is to be noted that for time varying flows J_{tot} is not constant; the implications of this on the definition of true bubble slip will be discussed later.

3. Results and discussion

In this section, results of heat transfer investigation during (i) isolated Taylor bubble flow and, (ii) pulsating Taylor bubble-train flow inside a single side heated square channel are discussed.

3.1. Heat transfer investigation of isolated Taylor bubble flow

In this study, the temperature trace of an isolated Taylor bubble flow on the heated wall of the square mini-channel of size

3.0 mm × 3.0 mm is quantified. Isolated air bubbles of various lengths are injected in the steady liquid water flow to observe the effect of air bubble length on the local heat transfer. When steady state is reached in single-phase liquid flow at a given flow rate, a single isolated Taylor bubble of air is injected in the liquid flow via the T-junction, which is located far upstream in the tube from the heated test section, as was shown in Fig. 1. This ensures that, any flow perturbations created by sudden injection of the bubble gets dissipated by the time this bubble reaches the heated test section.

Typical temporal and spatial temperature profiles of the heated wall with its corresponding IR thermograms captured by InfraRed Thermography at two different liquid flow Reynolds numbers have been shown in Fig. 2(a)–(f) In Fig. 2(a) and (d), temporal temperature response of heated wall at different axial locations is shown for two different liquid flow rates and with different bubble lengths. Fig. 2(a) correspond to liquid flow $Re \sim 110$, while Fig. 2 (d) correspond to liquid flow $Re \sim 55$. The digital images attached along with show the corresponding bubbles as injected into the channel, respectively, with the corresponding two-phase flow parameters. In all the experiments reported here, the flow Capillary number is of the order 10^{-4} and the relative slip m $(=(U_b - U_s)/U_b)$ is always less than 0.5.

The temperature footprints of the passing Taylor bubbles on the heated wall, at both the flow velocities, show some common features. It is observed that as the head of the air bubble reaches different axial locations in the heated zone of the flow, the local wall temperature immediately increases; this happens as it comes in contact with low thermal capacity air bubble. Subsequently afterwards, at the point of time when the tail of the air bubble passes

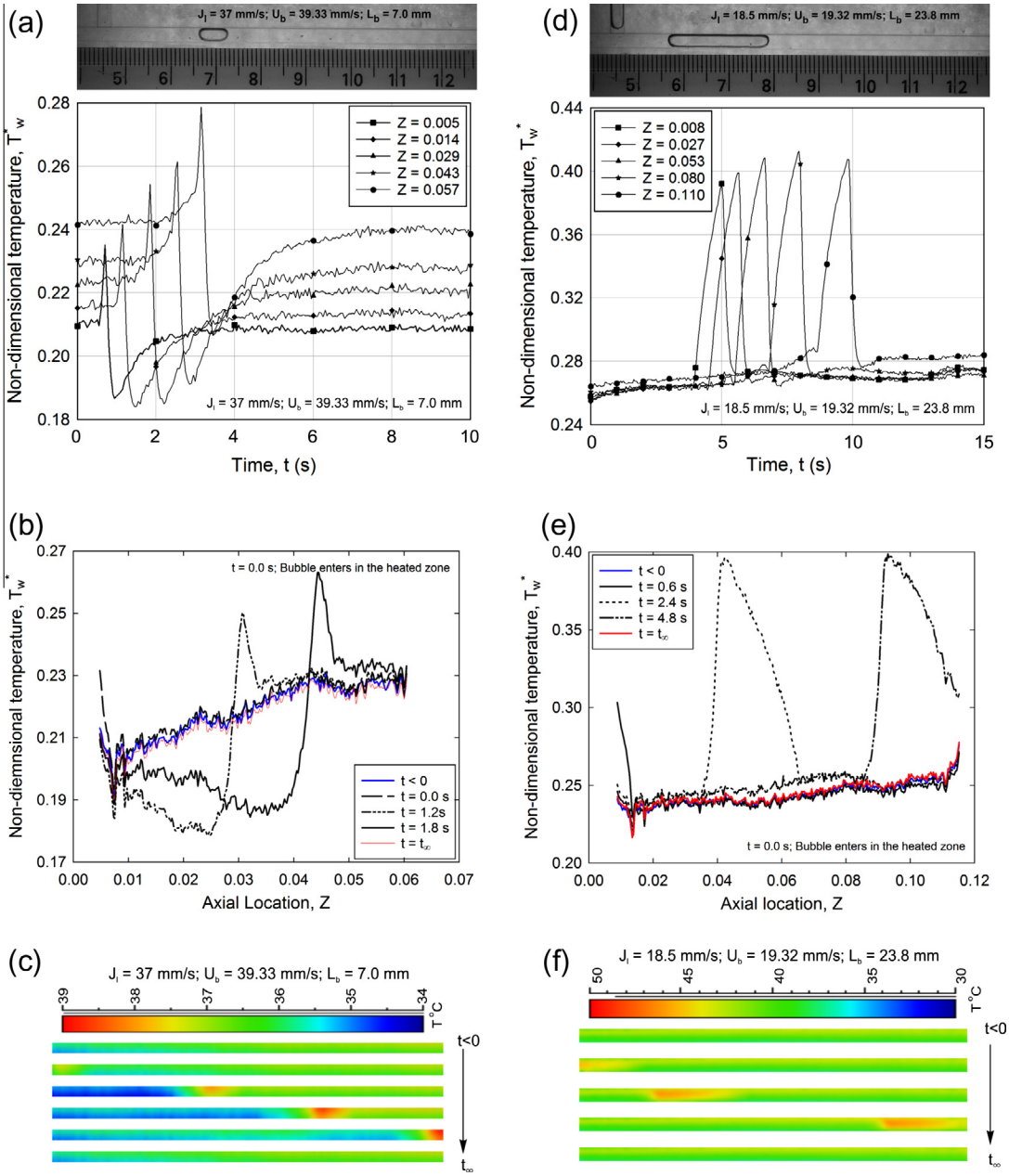

Fig. 2. (a) Temporal temperature response of heated wall at different axial locations for $Re = 110$. (b) Axial variation of heated wall temperature for $Re = 110$. (c) IR thermograms at different time instances for liquid $Re = 110$. (d) Temporal temperature response of heated wall at different axial locations for $Re = 55$. (e) Axial variation of heated wall temperature for $Re = 55$. (f) IR thermograms at different time instances for liquid Re = 55 [30].

over that Z-location thereby bringing the liquid phase to come in contact there, the local wall temperature sharply drops. As can be seen, this sharp drop of wall temperature is even below the corresponding steady-state value when only single-phase liquid was flowing, as shown in Fig. 2(a). The degree of this drop in wall temperature is such that it takes quite some time to come back to its original value corresponding to the steady-state liquid flow regime. As observed from the experimental data, this temperature regaining time is a function of liquid flow *Re*. This wall temperature variation behavior clearly shows that an isolated Taylor bubble passing in a liquid creates noteworthy flow disturbances in its wake region. This enhances the local liquid mixing in the bubble wake, resulting in the thinning of the thermal boundary layer and enhanced heat transfer.

It was also observed, as described in detail by the Mehta and Khandekar [30], that at any particular axial location along the flow, for a given liquid flow *Re*, the Taylor bubble length does not affect the drop in the local wall temperature significantly. This essentially indicates that, other flow parameters remaining the same, the wake region flow disturbances due to Taylor bubbles are quite independent of their length [30].

Due to the inherent constructional characteristics of the upstream T-junction, low liquid flow rate settings resulted in bubbles of longer lengths, as seen in Fig. 2(d), and corresponding instantaneous bubble images. The length of the bubble, as compared to the total length of the heated channel, has a clear impact on the local temperature footprint the bubbles generate. With bubbles of long lengths, the portion of heated flow zone covered by the low thermal capacity fluid (air) increases due to the larger residence time of the bubble inside the channel. Consequently, wall temperature increases to a much higher value. For this reason, the enhanced liquid mixing happening in the bubble wake, becomes quite ineffective in lowering the wall temperature to its original steady-state liquid flow value. This can be clearly seen in Fig. 2(d). The fact that every instance of Taylor bubble passage in the flow drops the local wall temperature in its wake region, suggests that for achieving continued augmentation of local heat transfer, injecting a series of small Taylor bubbles at regular intervals, thus dividing the liquid-phase into slugs of sufficiently smaller lengths, will be much more beneficial.

In addition, the axial variation of heater wall temperature (spatially averaged in *Y*-direction) during isolated Taylor bubble passage, as is shown in Fig. 2 (b) and (e) (which corresponds to the respective cases, earlier shown in Fig. 2(a) and (d)), for different time instances with its corresponding IR thermograms, highlights some interesting features. These temperature variations have also been compared with axial variation of temperature during steady-state single-phase liquid flow well before the bubble insertion ($t < 0$), and at sufficiently long time after the air bubble has left the heated channel ($t = t_\infty$).

It is evident from Fig. 2(b) that, when an isolated small bubble flows through the liquid flowing in the heated zone, it significantly lowers the heated wall temperature, as compared to its corresponding steady-state temperature value (when only liquid was flowing). On the other hand, when air bubble with longer lengths go in the heated zone (refer Fig. 2(e)), the wall temperature corresponding to the liquid flow steady-state value offers the minimum temperature value, i.e., the effect of longer bubbles in augmenting time averaged heat transfer is not significant. It can also be observed that the spatial thermal field of the heated wall is relatively less disturbed at the front of the bubble; however, at the rear end (tail) of the bubble, i.e., in its wake, the heated wall gets considerably cooled due to the effect of enhanced liquid mixing, which increases the heat transport rate from the wall. This signifies that, in comparison to the wake region behind the bubble tail, the fluidic disturbances in front of the bubble have lesser effect on the enhancement of local heat transfer. This situation is qualitatively quite analogous to flow over a solid bluff body (if we observe the flow from the frame of reference set onto the bubble). In such a situation too, major flow field disturbances are only seen in the wake region of the bluff body; the sharp temperature drop at the rear of the bubble is attributed to the local thermal disturbances caused due to local flow vortices [30]. In the front end, the flow stagnation caused by the bubble does not lead to heat transfer enhancement.

It can be inferred from the temperature footprints that injecting isolated Taylor bubbles into a steady flowing liquid significantly changes the local flow characteristics, thereby affecting the local thermal field; however, these flow disturbances are momentary and confined in nature, and therefore, after sufficiently long time following the passage of the Taylor bubble, the thermal situation returns back to the usual single-phase convective flow scenario. Hence, to sustain these disturbances and their ensuing advantage, continuous train of Taylor bubbles should be injected into the convective flow system. Local measurements of such flow (velocity contours and local spatial distribution of fluid temperature) must be attempted to resolve this phenomenon in more discernable details.

3.2. Heat transfer investigation of pulsating Taylor bubble-train flow

Enhancement of the heat transfer in isolated Taylor bubble-train flow over steady single-phase liquid flow has been clearly outlined in the previous section. However, whether this enhancement will further improve (or deteriorate) by externally applied flow frequency, as compared to the continuous Taylor bubble-train flow, needs to be addressed. In other words, the explicit contribution of flow pulsations in augmenting heat transfer, over and above what is achieved by steady Taylor bubbles, in Pulsating Heat Pipes needs to be scrutinized.

In this section, comparison of heat transfer investigation in continuous Taylor bubble-train flow (CTB) and pulsating Taylor bubble-train flow (PTB) is presented. The time-averaged flow rate in both the respective conditions becomes the natural choice for comparison of their heat transfer performances. In all the experiments, total superficial velocity J_{tot} (from 0.11 m/s to 0.15 m/s) was changed by varying the liquid flow rate, keeping the airflow rate constant. Broadly speaking, the choice of the range for J_{tot} was also motivated by typical flow rates encountered in PHPs. The liquid flow pulsating frequencies used in the PTB experiments were 1 Hz, 2 Hz and 3 Hz, which correspond to non-dimensional frequency parameter Wo = 3.4, 4.8 and 5.9, respectively, (alternately Strouhal number (St) can also be used, which only includes geometric and frequency parameter). Generally, as the frequency of oscillations in PHPs is limited to ~5 Hz [27,28], therefore, the experiments were performed at the three above-mentioned frequencies.

It is important to keep in mind, how pulsating Taylor bubbles got generated in the experimental set-up. As noted earlier, a T-junction was provided at the far upstream of the heated test section. In the liquid flow line (horizontal inlet) of T-junction, a solenoid valve arrangement was provided to make the liquid flow intermittent, as schematically shown in Fig. 3(a). The solenoid valve was triggered by an electronic timer circuit, which could be controlled to operate between 0 and 10 Hz. In the gas flow line connected to the T-junction (vertical inlet), flow of air was continuously available via a pressurized cylinder with controllable output via a humidifier. When both the phases met at the T-junction, bubbles were created because of the interaction of respective inertia forces of the phases, depending on their superficial velocities. Based on the results of isolated Taylor bubble flow reported in previous section, it can be argued that for a given flow rate of liquid and air, the local thermo-hydrodynamics will also depend

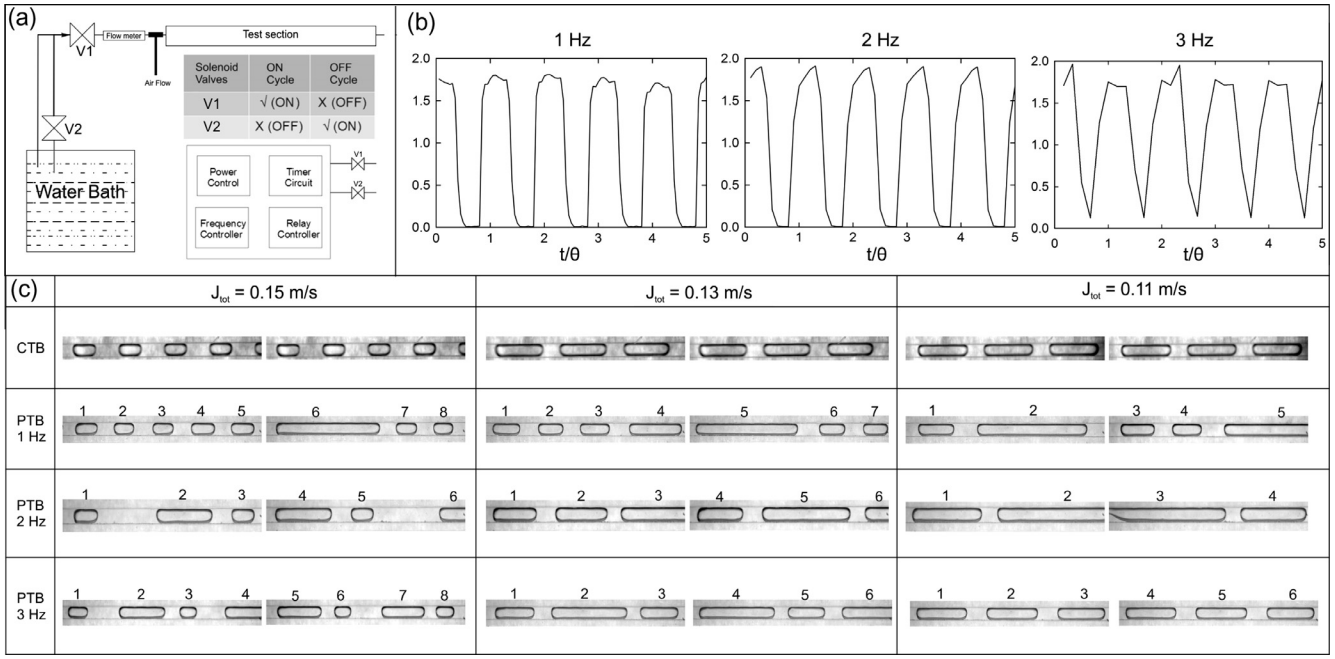

Fig. 3. (a) Schematic of the solenoid valve arrangement for generating PTB flow (b) The resulting liquid flow waveforms obtained by the solenoid arrangement during PTB flow (c) Images showing corresponding air-bubbles and liquid-slugs at various experimental conditions (CTB as well as PTB flow situations).

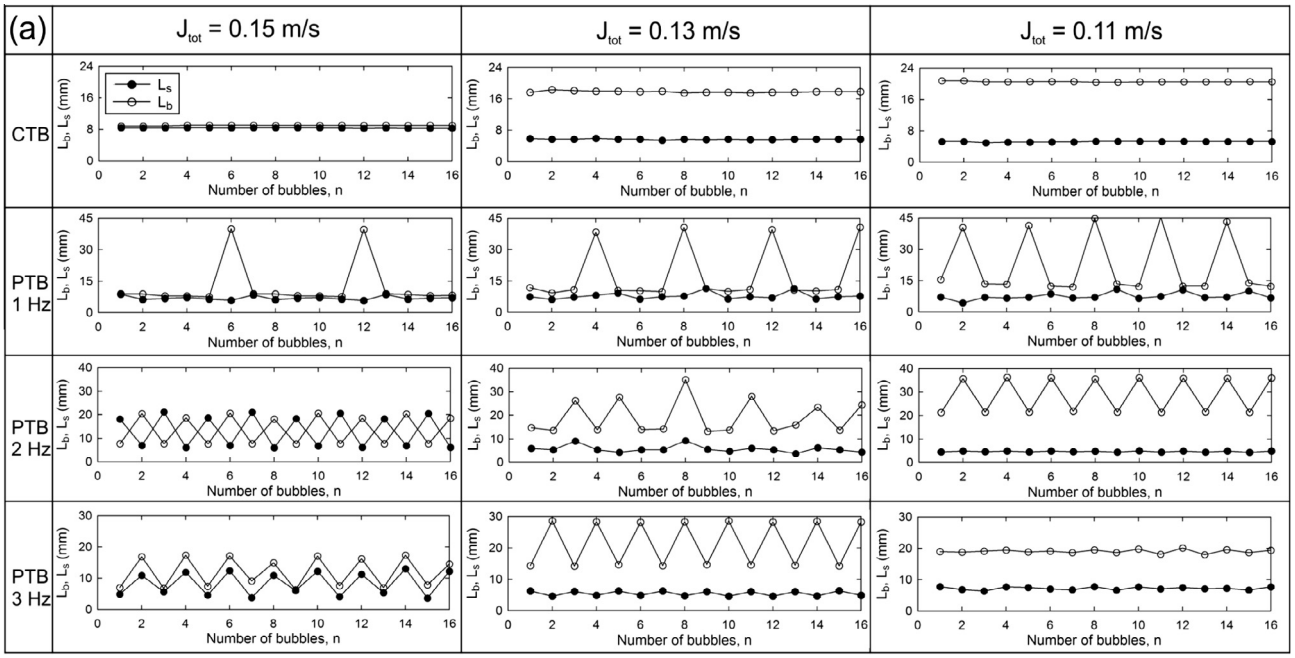

Fig. 4. Distribution of length of air-bubbles and liquid-slugs obtained by using the T-junction at various experimental conditions, corresponding to Fig. 5(c); the relevant flow parameters are summarized in Table 1; the number of bubbles shown in the abscissa represents the sequential Taylor bubbles tracked which travel one after the other during the train flow.

on the bubble-slug patterns, which get formed in the bubble-train formation process. However, due to the limitation of the T-junction method of generating Taylor bubbles, respective lengths of the bubbles and slugs could not be independently controlled; the pattern of bubble formation depended on the flow rates of individual phases and imposed flow pulsation frequency (in PTB flow). In other words, for a given liquid and air flow rates, there could have been other patterns of bubble-slug intermittency which could have been generated by some other bubble-formation/generation arrangement [23]. This essentially means that the heat transfer results presented here are broadly 'T-junction' specific; however, important conclusions on the thermal transport during such complex flows could be arrived at, as will be appreciated in the forthcoming sections. For the present T-junction, in both CTB/PTB flows, the repeatability of bubble-train pattern, for a given set of flow conditions was excellent. Representative sample photographs of the type of bubble-slug patterns, which got generated in the present experiments during CTB and PTB situation, under different flow

Table 1
Different flow variables used in Taylor bubble-train flow.

Time averaged gas flow rate Q_g (ml/min)	Time averaged liquid flow rate Q_l (ml/min)	Volume fraction β	Gas superficial velocity J_g (m/s)	Liquid superficial velocity J_l (m/s)	Total superficial velocity J_{tot} (m/s)	Two-phase Reynolds number Re_{TP}
50	30	0.624	0.093	0.057	0.15	444
50	20	0.714	0.093	0.037	0.13	388
50	9	0.833	0.093	0.017	0.11	333

rates of water and air, are shown in Fig. 3(c). Another way of representing the bubble-train data is shown in Fig. 4, wherein the lengths of individual bubble-slugs obtained under different operation conditions, corresponding to Fig. 3. Several interesting features of the ensuing flow pattern can be inferred from these two figures.

Referring to the CTB flow, the dimensions of the unit-cell generated by the T-junction depend on the total superficial velocity of the flow. As mentioned earlier, in this situation, the air flow rate was kept constant and the liquid flow rate was controlled to get the desired J_{tot}. The reduction in total superficial velocity resulted in longer air bubbles. The statistical quality of unit-cell dimensions (length of gas bubble, length of adjoining liquid slug and the bubble slip velocity) was excellent with standard deviations not exceeding 5%, of any given case. The T-junction performed quite satisfactorily in generating good quality, repeatable CTB flow.

Referring to PTB flow, the emerging flow patterns are more complicated as the imposed time scale of the flow pulsations changes the relative inertia forces of the two phases at the T-junction. This leads to a variety of bubble-slug combinational flow patterns, for a given set of flow conditions (the reported superficial velocity in this case is the time-averaged value over the pulsating cycle). As can be seen, in contrast to CTB flows, the unit-cell of PTB flow may have more than one bubble, but the formed patterns, for a given set of flow conditions, are repeatable. There is indeed a specific order in the distribution of bubbles and slugs in the 'unit-cell'. The statistical quality of repeatability of bubble-slug lengths is somewhat inferior as compared to the corresponding quality in CTB flow, but reasonably good with standard deviations of the order of 10–14% in unit-cell characteristics.

Fig. 5(a)–(c) shows the axial variation of time-averaged non-dimensional wall and fluid temperature for J_{tot} = 0.11 m/s, 0.13 m/s and 0.15 m/s, respectively, during CTB and PTB flow, the latter flow situation is at all three imposed frequencies. It is observed that time averaged wall temperature reduces with increased total superficial velocity. In addition, wall temperatures are also reducing when the flow is perturbed with higher frequencies (PTB flow at 2 Hz and 3 Hz) as compared to CTB flow. In contrast, wall temperature is higher for PTB flow at 1 Hz for all J_{tot} applied here. This behavior essentially indicates that, giving pulsations to the Taylor bubble-train flow may not be always advantageous as compared to the continuous Taylor bubble-train flow conditions.

It is known that in CTB flow, the average bubble velocity (U_b) is not equal to the total superficial velocity of the flow (J_{tot}), the ratio between the two is referred as the slip ratio (U_b/J_{tot}) [12]. Literature also suggests that the slip ratio itself is a function of the total superficial velocity [19] and hence, the flow Capillary number (Ca). In PTB flow, velocity of bubble moving inside the channel is not constant; it is varying with liquid flow. The hydrodynamics of the bubble wake is directly related to the relative velocity between the bubble and the liquid. Thus, it is reasonable to assume that bubble slip plays a role in the local heat transfer during both CTB and PTB flows. It is noted earlier that pulsating Taylor bubbles were generated by controlling the liquid flow rate and frequency. At lower imposed flow pulsating frequency, intermittent stop-over

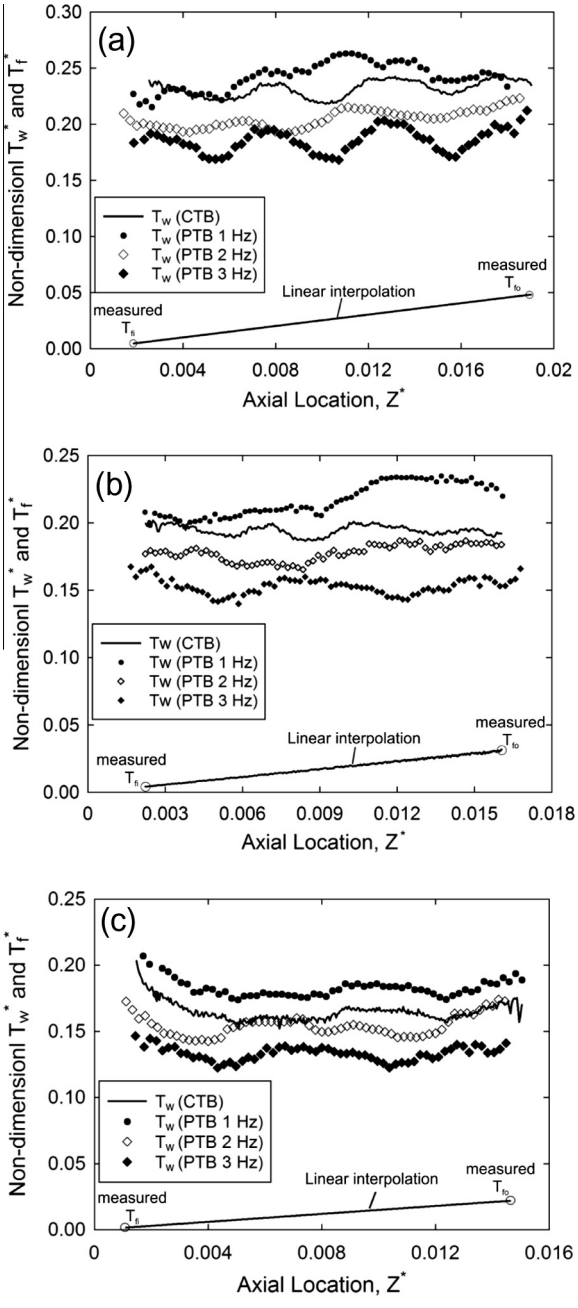

Fig. 5. Time averaged wall and fluid temperature for continuous Taylor bubble-train flow and pulsating Taylor bubble-train flow for 1 Hz, 2 Hz and 3 Hz (a) J_{tot} = 0.11 m/s (b) J_{tot} = 0.13 m/s (c) J_{tot} = 0.15 m/s, respectively.

time ('off-cycle') of the liquid-phase is large. Decelerating liquid flow correspondingly decelerates the flowing bubble-slug train in the downstream direction. Since the inertia of the two phases is different, this leads to a change in the local bubble slip. The reverse

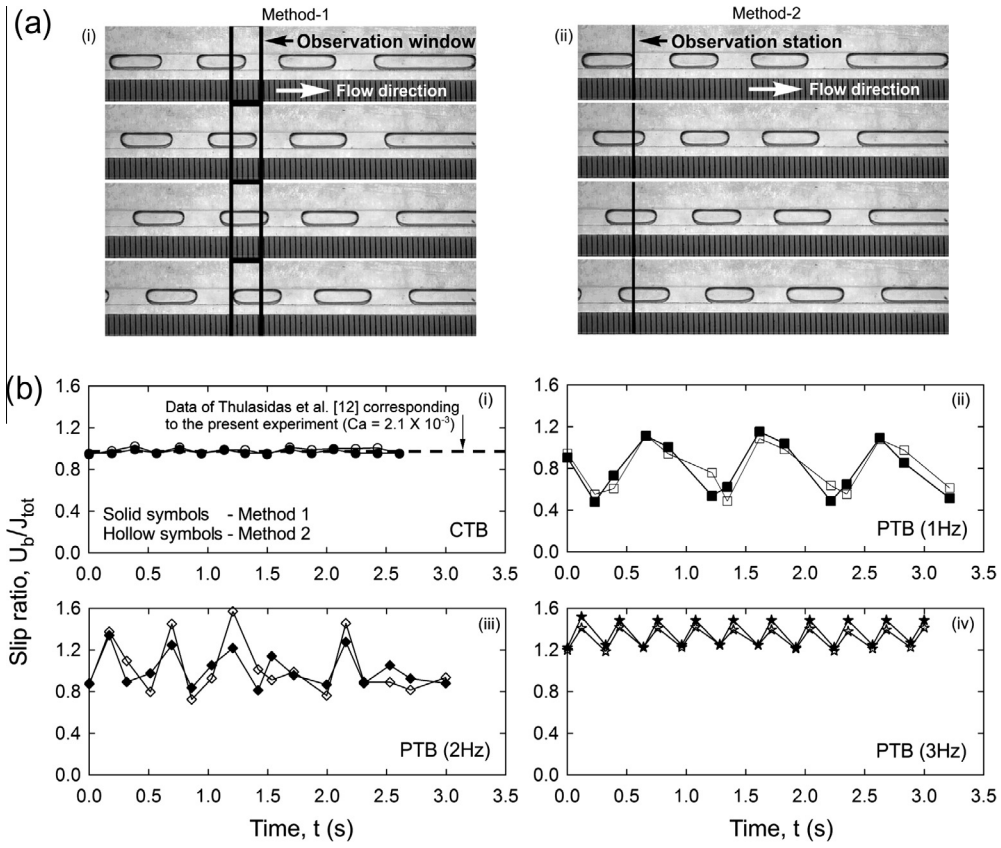

Fig. 6. (a) The two methodologies adopted for estimating the bubble velocity are depicted. (b) Variation of (U_b/J_{tot}) at J_{tot} = 0.13 m/s (Ca = 2.1 × 10^{-3}), as estimated from the two respective methods, for CTB and PTB flows.

phenomenon occurs when the liquid flow goes from the 'off-cycle' to the 'on-cycle'. Thus, pulsating liquid flow not only changes the bubble-slug length distribution but also affects the interfacial slip.

Determination of bubble slip under time varying Taylor flow conditions is challenging. True slip under such conditions can only be estimated if instantaneous local phase velocities of both the liquid and the gas phase, respectively, are known. However, when the Taylor flow is time varying, the denominator (J_{tot}) in the definition of slip is not constant. In other words, (U_b/J_{tot}) will not really represent the true instantaneous slip if time averaged value of J_{tot} is used. Thus, for PTB flows, the ratio does not have the same meaning as for CTB flows, unless the local instantaneous J_{tot} is used for estimation. In the present work, post processing of high speed digital videography data provided a good estimate of U_b but the flow instrumentation only provided an average value of J_{tot}.

Estimating U_b requires gathering of accurate positional coordinates of the bubble/menisci in a finite elapsed time period. This poses no special challenge (other than choosing the acquiring image capture rate of high-speed videography, which is dictated by the average superficial velocity) provided the bubble speed remains constant throughout the time window in which positional data is acquired. In other words, PTB flow poses yet another challenge in the estimation of instantaneous bubble velocity, as the total superficial velocity of the flow is continuously changing with time which affects instantaneous U_b.

Fig. 6(a) and (b) depicts the two independent strategies adopted in this work to estimate the ratio (U_b/J_{tot}) and its temporal variation, respectively. In Method-1 (Fig. 6(a)–(i)), a fixed observation window is chosen for the estimation of instantaneous bubble velocity, the intention being to estimate it by image processing, as the bubble passes through this observation window. As the studied flows are transient in nature (for PTB flow cases), therefore, the accuracy of calculation will depend on the of window size, frame rate and time period of imposed flow fluctuations. To get reasonable accuracy, the length (ℓ) of this chosen observation window should be such that the time scale calculated by ℓ/J_{tot} is sufficiently less than half of the time period of flow fluctuation ($\theta/2$). Further, the acquisition time between two consecutive digital images ($1/n$) should be at least an order of magnitude smaller than ℓ/J_{tot}. For the flows reported here, the observation window was typically of the order of ~5 mm. In such a window, the sequence of bubbles was tracked and time taken by a fixed designated point on the bubble (for example, the maxima/minima point on the bubble head/tail meniscus) to pass through the window was noted. Thus, dividing the length of the observation window by this traverse time, bubble velocities (U_b) were obtained.

In the second method of estimation (Method-2 in Fig. 6(a)–(ii)), bubble velocity is calculated by fixing a static 'point measurement station' on the acquired images. As the respective lengths of bubbles are known, the time taken by the entire bubble to cross that measurement station can therefore be estimated. In this case, the ratio of the bubble length to the time taken by bubble to cross the measurement station will give the bubble velocity. When flow is time varying, the bubble velocities change with time and therefore, depending on the length of the bubbles being tracked vis-à-vis the superficial velocity of the flow and imposed flow frequency, this method is prone to varying accuracy in velocity estimation. In other words, for only CTB flow, Method-2 will be as accurate as Method-1.

Temporal variation of ratio (U_b/J_{tot}) calculated by both the methods, are shown for CTB flow and PTB flow at different

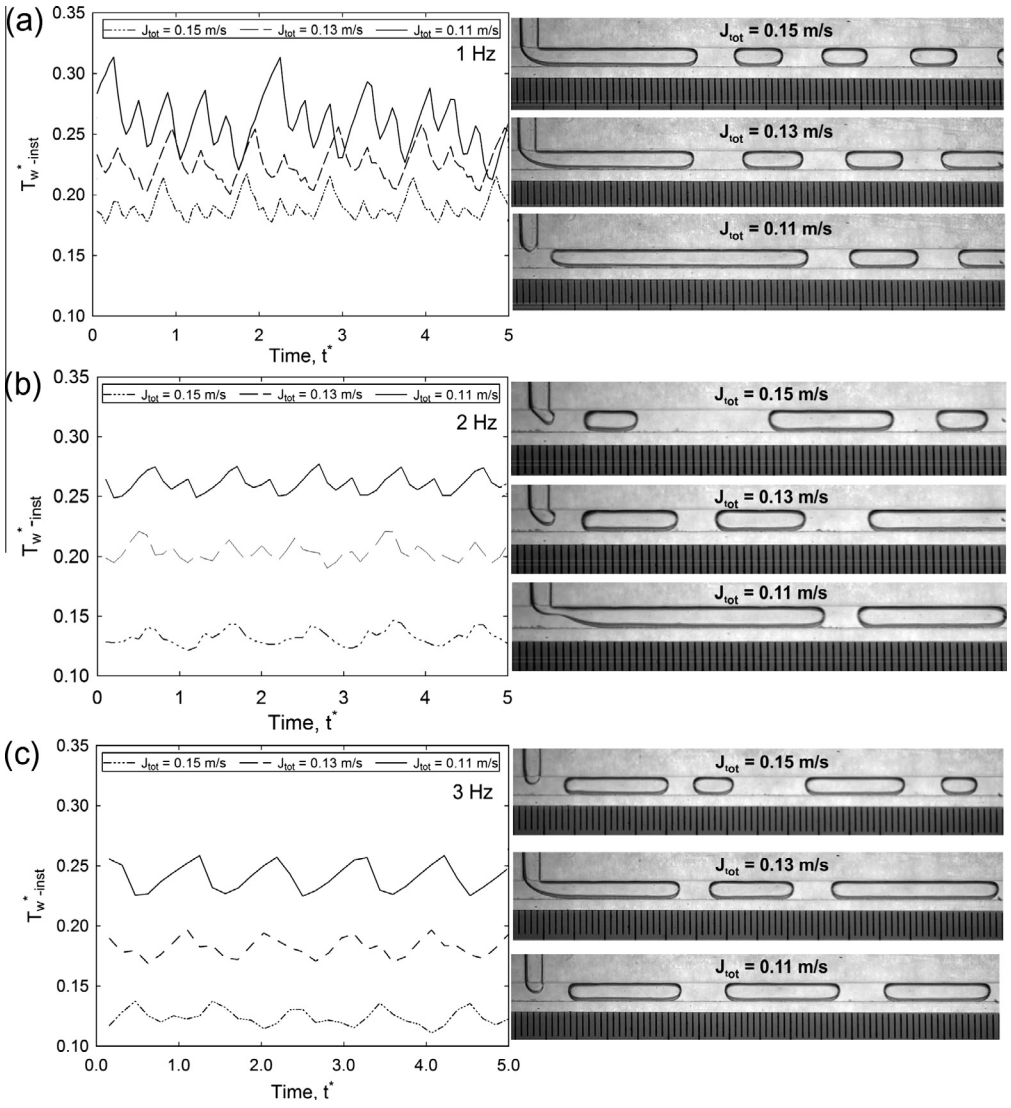

Fig. 7. Instantaneous wall temperature at Z^* = 0.01 and the corresponding image of local liquid slug-bubble distribution for (a) pulsating Taylor bubble-train flow at 1 Hz. (b) Pulsating Taylor bubble-train flow at 2 Hz. (c) Pulsating Taylor bubble-train flow at 3 Hz, respectively.

frequencies in Fig. 6(b).[2] As can be observed for CTB flows, the ratio (U_b/J_{tot}) which represents true slip for this case is nearly identical, as calculated by both methods. Further, the present data is very close to the data reported by Thulasidas et al. [12]. For PTB flows, as discussed earlier, this ratio does not truly represent the instantaneous slip; however, it provides important insight for comparison of heat transfer. It can be seen that the average values of (U_b/J_{tot}) increase with increasing flow frequency. Instantaneous bubble velocity is a direct function of liquid film thickness surrounding the Taylor bubble (or, in other words, the available area of cross section for the gas-phase), which, in turn, depends on the flow Capillary number (Ca) [12,15,17]. In addition, the presence of wall corners in non-circular channels plays a significant role in circumferential variation of film thickness. At lower phase velocities or low Ca, surface tension force dominates over the viscous forces (at low Ca inertia forces are anyway low) which results in larger film thickness at the corners than the central region of the wall. In the transient flow, when phase velocities are continuously changing with time, the film thickness also varies temporally. Consequently, U_b/J_{tot} is changing with time, which has been captured with the two methodologies described earlier. High frequency pulsations with repeated 'on' and 'off' cycles result in higher local acceleration/deceleration of fluid particles, which results in higher local (U_b/J_{tot}), as can be seen from the results. This leads to greater degree of bubble-wake perturbations, which eventually generates higher mixing in the adjoining liquid slugs [12,15,20], thereby enhancing transverse momentum and energy exchange and reducing the local wall temperature, as seen earlier in Fig. 5. Thus, high frequency PTB flows tend to perform better than corresponding CTB flows. In addition, it can also be seen that both the methodologies of slip estimation are comparable, with discrepancies in CTB flows much lower than the PTB flows, as expected, due to time-invariant nature of the former flow pattern.

Fig. 7 shows the instantaneous wall temperature at axial location Z^* = 0.01 and the corresponding local slug-bubble distribution

[2] It is to be noted that Fig. 6(b) is plotted on the premise that, at any given instance of time, the respective phase velocities of all the bubbles which constitute the Taylor bubble train are equal, by virtue of phase-incompressibility and no net mass transfer at the interface due to saturated conditions. By invoking these assumptions, estimation of temporal variation of bubble velocity, by either tracking a single bubble in time and space (for example, in Lagrangian frame), or tracking different bubbles at fixed Eulerian locations in space (as done in the present calculations by Method-1 and Method-2)) ought to be identical, except for the fact that in the former case, bubble velocity data will be continuous while in the later, the data are only obtained when bubble is passing through the measurement location/station.

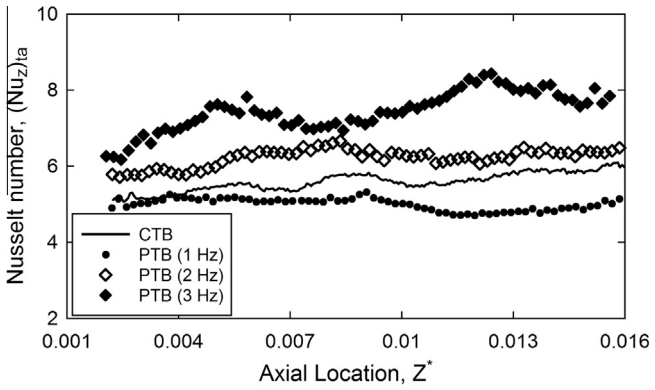

Fig. 8. Time-averaged Nusselt number for CTB and PTB at different frequencies at J_{tot} = 0.13 m/s; Nusselt number shown here are based on the bulk mean temperature estimated by interpolation of inlet and outlet measured fluid temperature by thermocouples.

for PTB flow. All the three imposed frequencies, at different values of applied J_{tot}, are depicted. In Fig. 7(a), for the entire range of J_{tot} (0.15–0.11 m/s), various peaks are observed in the wall temperature. These peaks are obtained at that location because of the passage of bubble-slug patterns, as shown in Fig. 3. When a bubble reaches a certain channel location, due to its low heat transfer capabilities, the wall temperature increases. This increase continues until a liquid slug reaches that location and cools it down. Qualitatively speaking, this phenomenon is similar to what was observed for isolated Taylor bubble flow, reported in Section 3.1. For this reason therefore, the absolute increase in the heater wall temperature is directly related to the length of gas bubbles. For example, for 1 Hz PTB flow frequency (where, as seen in Fig. 3(c), for all the three cases, a number of small bubbles are passing after a relatively long bubble), the increase in wall temperature, during the passage of the long bubble, is so high that the subsequent bubble-train section comprising of five smaller bubbles is not sufficient to cool down the wall. On the other hand, it has been observed that at higher frequencies (2 Hz and 3 Hz), the length of the longest bubble reduces, thereby changing the subsequent slug-bubble distribution, which favorably affects the heat transfer; this helps to keep the overall wall temperature at a lower value, as compared to the 1.0 Hz case.[3]

It is also obvious that heat transfer increases with increase in total superficial velocity. This is because (a) at higher J_{tot}, proportion of liquid-phase is higher, and (b) due to high liquid flow momentum, breakage of gas-phase occurs into larger number of smaller bubbles, as seen in sequence of images in Fig. 7. Thus, in the heated zone, sufficient amount of liquid-phase is present to convect the heat. As the liquid flow momentum decreases in the 'off-cycle', individual lengths of generated bubbles increase, which is observable from the instantaneous wall temperature plot in Fig. 7. In this case, overall proportion of liquid-phase in the heated zone decreases, which deteriorates the heat transfer. Thus, deterioration of heat transfer is observed with decrease in two-phase velocities, for all the cases discussed here.

Finally, it is interesting to observe the effect of imposed frequency on heat transfer. Fig. 8 shows the axial variations of time-averaged Nusselt number for CTB flow and PTB flow, respectively. In line with the wall temperature data presented in Figs. 5 and 7, it can be seen that heat transfer increases over CTB flow for higher frequency while it reduces for lower frequency. Thus, perturbing the Taylor bubble-train flow may conditionally lead to enhancement in the heat transfer in comparison to the continuous Taylor bubble-train flow. It is worth noting that to estimate the Nusselt number correctly, axial distribution of bulk mean temperature of the fluid should be known. Here, the axial variation of the fluid temperature is interpolated from the thermocouple measurements, done at the inlet and outlet of the channel.

The above set of results indicate that the length of the 'bubble-slug unit-cell', the local bubble slip and the overall superficial velocity of the flow are the three vital parameters which determine the heat transfer in CTB flows. The flow frequency is an additional parameter, which affects PTB flows. As noted earlier, bubble slip depends on J_{tot} and imposed flow frequency.

4. Summary and conclusions

Pulsating Heat Pipes are complex two-phase devices, which are characterized by self-sustained, thermally driven pulsating Taylor bubble flows. The heat transfer is a combination of latent heat and sensible heat, with the later dominating the net contribution. The flow physics is quite intricate and for proper understanding of the ensuing physics, there is a need to break down the problem into simpler sub-constituents such that their complex flow and heat transfer behavior can be eventually understood. Such an attempt has been done in this study wherein local thermo-hydrodynamics of non-boiling continuous and pulsating Taylor bubble flow has been studied.

In addition, many engineering applications in mini-/microscale require enhanced heat transfer characteristics from convective fluids. Under such geometrical constraints, the ensuing flows are typically laminar with limited heat transport capability. Introduction of simple non-boiling isolated Taylor bubbles and pulsating Taylor bubble-train in the flow can be an effective strategy for enhancement of local heat transfer, as reported in the present study.

The major conclusions of the study are as follows:

- Disturbing the single-phase liquid flow by injecting an isolated Taylor bubble, substantial drop (up to about 30%) in non-dimensional heated wall temperature that lies behind the bubble tail, is observed. This lower temperature zone exists for quite some time even after the bubble has passed. Length of the bubble, as compared to the total length of the heated channel, is an important parameter to achieve augmentation in the heat transfer. If bubble length is comparable to the heated zone, then the advantage in terms of heat transfer augmentation is lost.
- Heat transfer increases with increase in total two-phase velocities (J_{tot}) for both continuous Taylor bubble-train (CTB) and pulsating Taylor bubble-train (PTB). Imposition of pulsations on CTB may enhance the heat transfer; the degree of enhancement is intrinsically linked with not only the imposed flow frequency but also the local phase distribution. PTB at higher frequencies studied here, i.e., at 2 Hz and 3 Hz showed better heat transfer characteristics than the CTB and PTB at 1 Hz because of increased bubble velocity at the interface as well as change in the phase-distribution.
- Estimation of bubble slip in time varying or pulsating Taylor bubble train flows is challenging. Two methodologies to capture bubble velocity by digital image processing, having independent statistical approach, were presented and compared. Choosing the appropriate parameters for post processing of the data, vis-à-vis the flow parameters of the time varying flow under scrutiny is critical in correct estimation of the bubble slip for such flow conditions.
- In the background of results obtained from the present research, some clear insights into the functioning of PHPs can be given.

[3] As has been noted earlier, due to the specific design constraint of the T-junction, explicit and separating effects of the two parameters, i.e., pulsating frequency and bubble-slug distribution, could not be achieved in this study.

- Net heat throughput in a PHP is a combination of evaporation/condensation, by the bubbles (latent heat contribution) and oscillating movement of liquid slugs (sensible heat transport). It is already a known fact that the latter, i.e. sensible heat transfer is the major contributor. This indicates that liquid slug distribution is one of the important parameter for improving thermal performance of PHPs. The sensible heating/cooling transport capability of the liquid slugs can be altered by controlling the wake generated by the adjoining Taylor bubbles. The liquid slug/vapor bubble lengths depend on the initial filling charge ratio of the PHP. This partly explains the reason of low performance at high filling ratio, when length of liquid slugs is higher. The present research clearly suggests that smaller bubble/slug train will be beneficial.
- It is also inferred by the present results that higher the frequency of flow oscillations, higher will be the thermal performance of the PHPs. In fact, this is corroborated by the experimental results of PHPs available in the open literature. Higher operating flow frequencies will increase the bubble slip and enhance the mixing in the adjoining liquid slugs.
- The present results also indicate that the length of bubbles as compared to the total length of the evaporator/condenser also plays a role in the overall heat transfer performance of PHPs.
- It is also deduced from the present results that unless a thorough understanding of all the applicable time scales of the system dynamics are discerned, progress in modeling of PHPs cannot be accomplished. In addition, most literature reporting system level dynamics of PHPs do not consider the conjugate nature of heat transfer which may substantially change the local dynamics. Unless conjugate effects are quantified, true and meaningful, performance characteristics of the system cannot be established.

Conflict of interest

None declared.

Acknowledgment

Financial grants from the Indo-French Center for Promotion of Advanced Research (IFCPAR), New Delhi, India (Project #4408-1) are gratefully acknowledged. The Infrared camera was procured under the FIST funding scheme of the Department of Science and Technology, Government of India.

References

[1] H. Akachi, US patent, Patent number 4921041, 1990.
[2] H. Akachi, F. Polášek, P. Štulc, Pulsating heat pipes, in: Proceedings of Fifth International Heat Pipe Symposium, Melbourne, Australia, 1996.
[3] S. Khandekar, M. Groll, An insight into thermo-hydraulic coupling in pulsating heat pipes, Int. J. Therm. Sci. 43 (1) (2004) 13–20.
[4] L.L. Vasiliev, Heat pipes in modern heat exchangers, Appl. Therm. Eng. 25 (2005) 1–19.
[5] Y. Zhang, A. Faghri, Heat transfer in a pulsating heat pipe with open end, Int. J. Heat Mass Transfer 45 (2002) 755–764.
[6] H. Zhang, A. Faghri, Advances and unsolved issues in pulsating heat pipes, Heat Transfer Eng. 29 (1) (2008) 20–44.
[7] D. Spernjak, A.K. Prasad, S.G. Advani, Experimental investigation of liquid water formation and transport in a transparent single-serpentine PEM fuel cell, J. Power Sources 170 (2007) 334–344.
[8] L. Tadrist, Review on two-phase flow instabilities in narrow spaces, Int. J. Heat Fluid Flow 28 (2007) 54–62.
[9] S.P. Das, V.S. Nikolayev, F. Lefevre, B. Pottier, S. Khandekar, J. Bonjour, Thermally induced two-phase oscillating flow inside a capillary tube, Int. J. Heat Mass Transfer 53 (2010) 3905–3913.
[10] M. Rao, F. Lefevre, S. Khandekar, J. Bonjour, Understanding transport mechanism of a self-sustained thermally driven oscillating two-phase system in a capillary tube, Int. J. Heat Mass Transfer 65 (2013) 451–459.
[11] J. Fabre, A. Liñe, Modeling of two-phase slug flow, Annu. Rev. Fluid Mech. 24 (1992) 21–46.
[12] T.C. Thulasidas, M.A. Abraham, R.L. Cerro, Bubble train flow in capillaries of circular and square cross section, Chem. Eng. Sci. 50 (1995) 183–199.
[13] T.C. Thulasidas, M.A. Abraham, R.L. Cerro, Flow patterns in liquid slugs during bubble train flow inside capillaries, Chem. Eng. Sci. 52 (17) (1997) 2947–2962.
[14] T. Taha, Z.F. Cui, Hydrodynamics of slug flow inside capillaries, J. Chem. Eng. Sci. 59 (2004) 1181–1190.
[15] T. Taha, Z.F. Cui, CFD modeling of slug flow inside square capillaries, Chem. Eng. Sci. 61 (2006) 665–675.
[16] M.N. Kashid, I. Gerlach, S. Goetz, J. Franzke, J.F. Acker, F. Platte, D.W. Agar, S. Turek, Internal circulation within the liquid slugs of a liquid–liquid slug-flow capillary microreactor, Ind. Eng. Chem. Res. 44 (2005) 5003–5010.
[17] C.Q. Yao, Y.C. Zhao, C.B. Ye, M.H. Dang, Z.Y. Dong, G.W. Chen, Characteristics of slug flow with inertial effects in a rectangular microchannel, Chem. Eng. Sci. 95 (2013) 246–256.
[18] J. Yue, L. Luo, Y. Gonthier, G.W. Chen, Q. Yuan, An experimental study of air–water Taylor flow and mass transfer inside square microchannels, Chem. Eng. Sci. 64 (16) (2009) 3697–3708.
[19] Q. He, Y. Hasegawa, N. Kasagi, Heat transfer modelling of gas–liquid slug flow without phase-change in a micro tube, Int. J. Heat Fluid Flow 31 (2010) 126–136.
[20] A.K. Bajpai, S. Khandekar, Thermal transport behavior of a liquid plug moving inside a dry capillary tube, Heat Pipe Sci. Technol. 3 (2–4) (2012) 97–124.
[21] Z.Y. Bao, D.F. Fletcher, B.S. Haynes, An experimental study of gas liquid flow in a narrow conduit, Int. J. Heat Mass Transfer 43 (2000) 2313–2324.
[22] C. Narayanan, D. Lakehal, Two phase convective heat transfer in miniature pipes under normal and micro-gravity conditions, ASME J. Heat Transfer 130 (2008) 074502.
[23] R. Gupta, D.F. Fletcher, B.S. Haynes, CFD modelling of flow and heat transfer in the Taylor flow regime, Chem. Eng. Sci. 65 (2010) 2094–2107.
[24] A.P. Walsh, J.E. Walsh, S.Y. Muzychka, Heat transfer model for gas–liquid slug flows under constant flux, Int. J. Heat Mass Transfer 53 (2010) 3193–3201.
[25] A. Majumder, B. Mehta, S. Khandekar, Local Nusselt number enhancement during gas–liquid Taylor bubble flow in a square mini-channel: an experimental study, Int. J. Therm. Sci. 66 (2013) 8–18.
[26] B. Mehta, S. Khandekar, Measurement of local heat transfer coefficient during gas–liquid Taylor bubble train flow by infrared thermography, Int. J. Heat Fluid Flow 45 (2014) 41–52.
[27] J.L. Xu, Y.X. Li, T.N. Wong, High speed flow visualization of a closed loop pulsating heat pipe, Int. J. Heat Mass Transfer 48 (2005) 3338–3351.
[28] S. Khandekar, A.P. Gautam, P.K. Sharma, Multiple quasi-steady states in a closed loop pulsating heat pipe, Int. J. Therm. Sci. 48 (2009) 535–546.
[29] M. Mameli, M. Marengo, S. Khandekar, Local heat transfer measurement and thermo-fluid characterization of a pulsating heat pipe, Int. J. Therm. Sci. 75 (2014) 140–152.
[30] B. Mehta, S. Khandekar, Footprint of isolated Taylor bubble on wall temperature of a horizontal square mini-channel, in: Paper # HMTC1300650, Proc. 22th National and 11th International ISHMT-ASME Heat and Mass Transfer Conference, December 28–31, 2013, IIT Kharagpur, India.